

# EXPLAINING THE OBSERVED VELOCITY DISPERSION OF DWARF GALAXIES BY BARYONIC MASS LOSS DURING THE FIRST COLLAPSE

MATTHIAS GRITSCHNEDER<sup>1,2</sup>, DOUGLAS N.C. LIN<sup>1,2</sup>

<sup>1</sup> Astronomy and Astrophysics Department, University of California, Santa Cruz, CA 95064, USA

<sup>2</sup>Kavli Institute for Astronomy and Astrophysics, Peking University, Yi He Yuan Lu 5, Hai Dian, 100871 Beijing, China

*Draft version January 16, 2013*

## ABSTRACT

In the widely adopted  $\Lambda$ CDM scenario for galaxy formation, dwarf galaxies are the building blocks of larger galaxies. Since they formed at relatively early epochs when the background density was relatively high, they are expected to retain their integrity as satellite galaxies when they merge to form larger entities. Although many dwarf spheroidal galaxies (dSphs) are found in the galactic halo around the Milky Way, their phase space density (or velocity dispersion) appears to be significantly smaller than that expected for satellite dwarf galaxies in the  $\Lambda$ CDM scenario. In order to account for this discrepancy, we consider the possibility that they may have lost a significant fraction of their baryonic matter content during the first infall at the Hubble expansion turnaround. Such mass loss arises naturally due to the feedback by relatively massive stars which formed in their centers briefly before the maximum contraction. Through a series of N-body simulations, we show that the timely loss of a significant fraction of the dSphs initial baryonic matter content can have profound effects on their asymptotic half-mass radius, velocity dispersion, phase-space density, and the mass fraction between residual baryonic and dark matter.

*Subject headings:* Methods: numerical, Galaxies: dwarf, Galaxies: evolution, Galaxies: structure, (Cosmology: ) dark matter

## 1. INTRODUCTION

Dwarf galaxies play an important role in the  $\Lambda$ CDM scenario for galaxy formation. They form early, in relatively dense background environments, and are the building blocks of larger galaxies.  $\Lambda$ CDM simulations show that these dwarf galaxies retain their integrity during their merger process and predict a rich population of satellite dwarf galaxies around large galaxies such as the Milky Way (e.g. Diemand et al. 2008; Springel et al. 2008).

Many satellite dwarf spheroidal galaxies (dSphs) in the Galactic halo have been found through SDSS and other surveys. Follow-up spectroscopic observations reveal these dSphs are surrounded by dark-matter halos. But, the internal phase space density of the most newly discovered (faint) satellite dSphs is significantly smaller than that predicted from the dark-matter-only simulations. This discrepancy poses a challenge to the standard  $\Lambda$ CDM scenario in its simplest form (e.g. Boylan-Kolchin et al. 2011; Ferrero et al. 2011; Rashkov et al. 2012; Boylan-Kolchin et al. 2012; Wolf & Bullock 2012). Recent observations show that this problem is not limited to the Milky Way, but present in Andromeda as well (e.g. Tollerud et al. 2012).

We examine the dSphs' structural adjustment associated with the loss of baryonic matter due to star formation feedback. Today, the dSphs' total dark to baryonic matter ratio is generally much larger than the corresponding cosmological value (Mateo 1998). The preferential loss of baryonic matter may be the potential solution to both the "missing baryonic matter" and the "missing satellite" (e.g. Klypin et al. 1999; Moore et al. 1999) puzzles.

There is very little detectable molecular or atomic gas inside the dSphs today. In §2, we briefly discuss the possibility that a significant fraction of the initial gas content may be lost due to the feedback effect of first generation stars in them. Presumably, this effect is most intense during the collapse following the dSph progenitors' turn around from the Hubble flow. We show, in §3, how the loss of a small fraction of the total mass may significantly affect dSphs' asymptotic dynamical structure. Baryonic matter may also be removed from the dSphs through tidal or ram pressure stripping by tenuous gas in the Galactic halo (Lin & Faber 1983). However, gradual loss of gas from the dSphs' virialized potential would not significantly affect their internal dynamical structure.

There have been several attempts to include baryonic matter in comprehensive cosmological simulations of galaxy formation (Gnedin et al. 2009). For computational efficiency, a simple-to-use prescription for star formation rates (as a function of local gravity, gas density, temperature, metallicity, and background radiation) is clearly technically desirable. However, there are many competing effects including atomic processes, radiation transfer, hydrodynamics and magnetic fields, which are sensitive to the diverse initial and boundary conditions over a large dynamic range in spacial extent and time scales. The determining factors for the onset, efficiency, and impact of star formation remain enigmatic.

If the present-day stellar content is distributed widely in the form of initial gas through dSphs, the background UV flux after the epoch of re-ionization would easily ionize the gas within typical dwarf galaxies, delaying or even preventing cooling and star formation within them (Dong et al. 2003; Brown et al. 2012). Most dSphs within the Local Group are observed to contain multiple generations of stars, the oldest of which formed in the

early epochs of cosmic evolution, when the background UV flux may have been intense. Possible solutions to this conundrum include that the formation of these stars preceded the epoch of re-ionization or that these dSphs may have lost most (up to  $\sim 90\%$ ) of their original baryonic content which provided a more effective shield against external UV photons. The second possibility is in line with the large mass ratio between dark and baryonic matter in dSphs.

Most recent cosmological simulations (Brooks & Zolotov 2012; Governato et al. 2012) produce results which appear to be in agreement with our baryonic mass loss conjecture. It has also been argued that about 10% of the haloes in simulations might not face the 'too big too fail' problem (Purcell & Zentner 2012). However, this conjecture only shifts the problem at hand towards the uniqueness of the Milky Way. Here, we present an idealized toy model for the formation of dSphs. We introduce a prescription to link the loss of the interstellar medium with the burst of first generation star formation in dSphs. The main advantage of our approach here is that it enables us to identify the key physical effects which determine dSphs' asymptotic dynamical structure. On the technical side, it also provides adequate resolution on the scale of the dSphs.

We first review, in §2, the basic assumptions, methodology, initial and boundary conditions used in our numerical models. We then continue to present the results of our dimensionless simulations (§3). In §4 we convert these numbers to physical quantities and in §5 we draw the conclusions.

## 2. BASIC APPROACH AND INITIAL CONDITIONS

The main cause of the loss of ordinary matter may be feedback associated with star formation. In previous simulations (Dong et al. 2003) on the effects of radiative transfer and photoionization in dSphs, it was shown that star formation can indeed proceed in their more massive and gas rich progenitors. The star formation and gas retention efficiency may vary widely in galaxies with similar dark matter potentials because they depend on many factors, such as the baryonic fraction, external perturbation, initial mass function, and background UV intensity. The presence of very old stars in dSphs indicates that their initial baryonic-to-dark matter content was comparable to the cosmic value. This constraint suggests that the initial density fluctuation of baryonic matter may be correlated with that of the dark matter. For the more massive dwarf elliptical galaxies, the star formation efficiency and gas retention rate are much higher. Their mass-to-light ratio is regulated by star formation feedback and is expected to be nearly independent of their absolute luminosity. The results of our theoretical models reproduce the observed  $(M/L) - M_V$  correlation (Mateo 1998).

Many dwarf galaxies contain stars with diverse  $[\text{Fe}/\text{H}]$  and some contain multiple generations of stars, including a recent ( $\approx$  Gyr) episode in the Fornax dSph (de Boer et al. 2012). Significant iron dispersion in dSphs suggests they were self contaminated by the retained and recycled supernova ejecta from massive stars. But, the total metal content in these systems is much less than expected from the heavy-element production of massive stars in each episode of star formation. Such

a deficiency implies that a substantial fraction of the dSphs' gravitational potential is generally shallow with a modest velocity dispersion. The UV flux from a few massive supernova- progenitor stars would be adequate to ionize the residual gas and evaporate it from the dSphs (Noriega-Crespo et al. 1989). In the presence of an initially disturbed gas distribution (due to photoionization), only a few percent of the gas enriched by the supernovae remains in the center of dSphs (Fragile et al. 2003).

The ionization and supernova blast wave only directly affect the dynamics of baryonic matter. Although the ejection speed may substantially exceed the escape speed of the dSphs' dark matter halo, the loss of baryonic matter makes small fractional changes in their total mass and potential. If this mass loss occurs after the dark matter halo has already virialized, it will only modify the dark matter content by a small amount. However, we are able to show here that a timely loss of baryonic matter during the virialization process would lead to an extended halo structure which is prone to subsequent harassment.

During the initial infall of the dSphs, both dark and baryonic matter attain infall velocities comparable to their escape speed before virialization. In the absence of any feedback, the gravity of the dark matter potential accelerates both components to attain a kinetic energy which is slightly less than their gravitational energy. As the density of both dark and baryonic matter increases, gas in the dSphs become self shielded against the background UV radiation. Thermal instability leads to the formation of dense cores and young stars. Photoionization and supernovae feedback induces the ejection of gas from the central regions of dSphs. At this advanced stage of infall, the total energy of the infalling dark and baryonic matter is a small fraction of the instantaneous potential energy (Aarseth et al. 1988) and a small fractional mass loss could offset the near cancellation between the kinetic and potential energy.

We consider the effect of baryonic matter loss on the evolution of the dark matter halo in dSphs, especially during the infall stage of their formation. In order to illustrate this effect, we consider a series of N-body simulations with the publicly available SEREN code (Hubber et al. 2011). The dark and baryonic matter is represented by 10000 particles which only interact with each other through their mutual gravity. For computational simplicity, we represent the Hubble expansion turn around with systems of particles at rest with a uniform initial density.

The system contracts under its own gravity. By reducing the mass of individual particles, we impose an instantaneous loss of a prescribed fraction  $f$  of the total mass after the half mass radius  $R_{\text{hm}}$  of the systems has reduced to  $R_{\text{loss}}$  from their original total radius  $R_0$  by a factor up to 20 (see §3). Our goal is to determine the asymptotic structure of the systems after virialization as a function of  $f$  and  $R_{\text{loss}}$ . Therefore, we need to generate models with the minimum value of  $R_{\text{hm}} < R_{\text{loss}}$ .

The minimum value of  $R_{\text{hm}}/R_0$  is determined by the initial fluctuation spectrum. For systems represented by N particles, its value, due to the global random noise, is  $\sim N^{-1/3}$  (Aarseth et al. 1988). This contraction factor would be limited in cosmological simulations with inadequate resolution on the scale of dSphs. For the entire

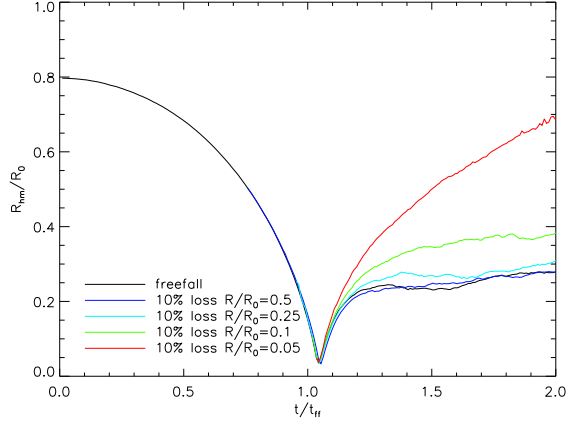


FIG. 1.— Dependence of the half-mass radius on the precise time of loss for different times of loss, characterized by the contraction of the halo at the time of the loss. We plot the radius in units of the initial radius and the time in units of the free-fall time.

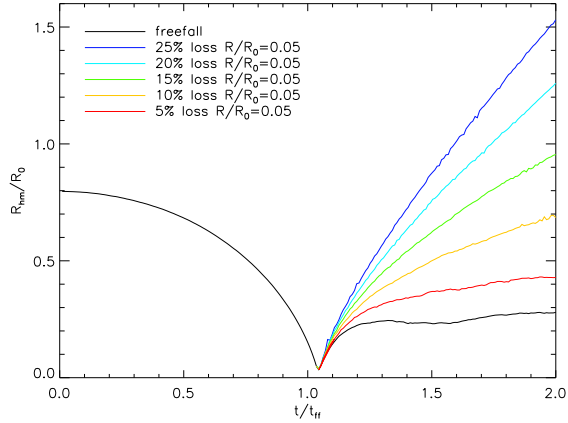


FIG. 2.— Dependence of the half-mass radius on the amount of loss for cases with a loss between 5% to 25% of mass loss. We plot the radius in units of the initial radius and the time in units of the free-fall time.

range of models in §3, it is adequate to use  $N = 10^4$ . Although the minimum value of  $R_{\text{hm}}/R_0$  may reduce with larger values of  $N$ , the asymptotic structure is affected by the global changes in the gravitational potential rather than two body relaxation process (i.e. it is determined by the values of  $f$  and  $R/R_0$  rather than  $N$ ).

For a fiducial model, we neglect any mass loss. In this case, the system relaxes into a virial equilibrium after a few times of its initial free fall time scale  $t_{\text{ff}}$ . A small fractional mass loss, especially during the advanced stage of the infall, can lead to much more extended relaxed kinematic structure after violent relaxation. We run the model for  $2t_{\text{ff}}$ , which is sufficient to reach a stable half mass radius in the fiducial case.

### 3. RESULTS

Here, we investigate a number of different scenarios. We vary the precise time of the mass expulsion, the amount of mass ejected as well as the region where the mass is expelled.

First, we investigate the timing of the loss. We investigate cases with a contraction to  $1/2$ ,  $1/4$ ,  $1/10$  and  $1/20$

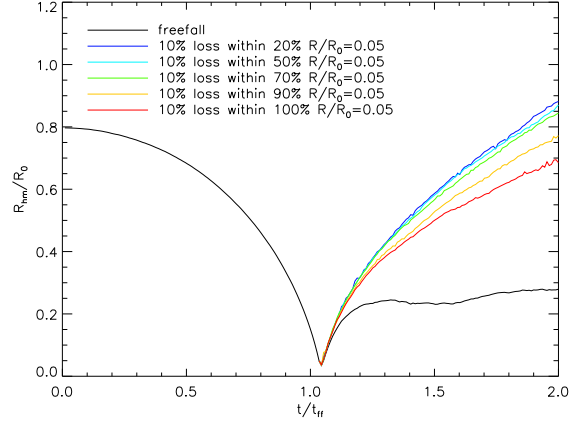


FIG. 3.— Dependence of the half-mass radius on the region of loss. 10% of the material is lost in to within a range of different regions. We plot the radius in units of the initial radius and the time in units of the free-fall time.

at the epoch of the mass loss, respectively. The corresponding dynamical timescales (to bounce back) are  $0.35t_{\text{ff}}$ ,  $0.13t_{\text{ff}}$ ,  $0.03t_{\text{ff}}$ , and  $0.01t_{\text{ff}}$ . From Figure 1 it becomes clear the timing is of crucial importance. The closer the loss to the maximum contraction, the more drastic the effect of baryonic mass loss on the entire dark matter halo. From a physical point of view, the first burst of star formation and thus the most efficient feedback is indeed to be expected at the first time high densities are reached, i.e. close to maximum contraction.

Another interesting feature is the amount of mass loss needed. Clearly, this parameter is strongly constrained by cosmological parameters, i.e. the maximum mass loss is limited by the amount of baryonic matter initially. According to WMAP7 (Komatsu et al. 2011), the ratio of baryonic to dark matter is about 1:4.45. Assuming this ratio is preserved in the initial halo, there is about 17% baryons inside the halo. We investigate a series of cases with an loss of 5% to 25%. Above 25% mass loss the halo disperses. Figure 2 shows a linear dependence of the final half-mass radius on the amount of mass loss (as expected from e.g. Aarseth et al. 1988). An encouraging result is that even the loss of about 10% of the total mass (i.e. slightly more than half of the baryonic mass) leads to a significant puff up, resulting in an halo twice as big as in the fiducial case.

In the context of the observed  $(M/L) - M_v$  relation and the final ratio of baryonic to dark matter of about 1:100 (e.g. Jardel & Gebhardt 2012), an even higher fractional mass loss ( $\sim 15\%$ ) is desirable. However, here we consider only a loss of 10% during the first infall, which is sufficient to explain the low phase-space density. The observed mass to light ratio is most likely later achieved via star bursts or tidal effects.

To increase the applicability of this numerical experiment to the problem at hand, it is important to constrain the region where the mass loss occurs. In a dwarf galaxy, the mass loss is only going to happen in the dense central region, where the baryons are going to form stars and subsequently remove the gas via their feedback. We simulate this effect by reducing mass of individual particles in a central fraction of the system. The results in Figure 3 show that a more centralized mass loss leads

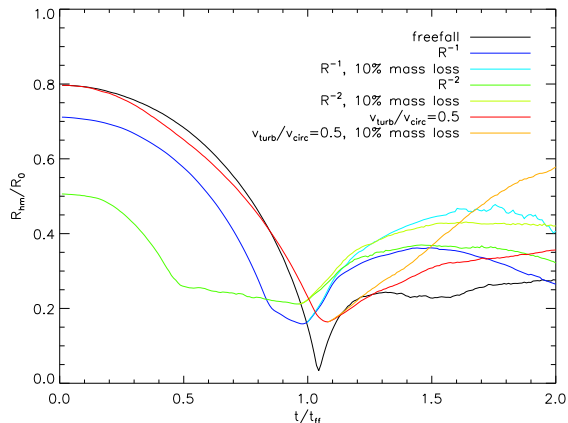


FIG. 4.— Evolution of the half-mass radius for initial conditions with a cusped profile ( $R^{-1}$  and  $R^{-2}$ ) or a turbulent velocity, respectively.

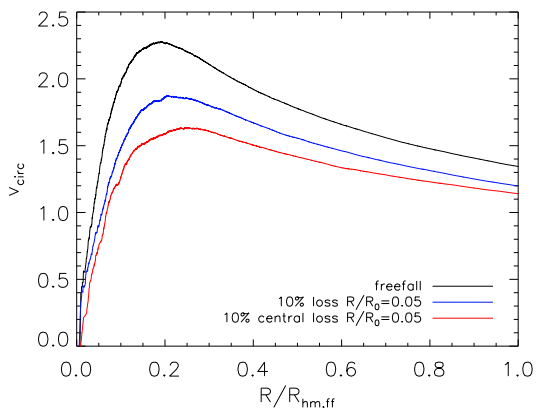


FIG. 5.—  $v_{\text{circ}}$ , i.e. the potential in three selected cases. We plot the velocity in code units versus the radius in units of the final half-mass radius in the fiducial, undisturbed case.

to a more extended asymptotic structure and makes the model more relevant for the formation of dwarf galaxies. As the dependence on the mass loss region is not sensitive, it merely demonstrates that an extended virialized system, as observed today, does not require mass loss to take place throughout the halo.

Recent cosmological simulations (e.g. Diemand & Kuhlen 2008) show that dwarf galaxies form from the inside out, as in the classic secondary infall model (Fillmore & Goldreich 1984; Bertschinger 1985). To test the validity of our model in this context we investigate the collapse of a cusped profile. We set up two profiles, corresponding to  $\rho \propto R^{-1}$  and  $\rho \propto R^{-2}$ , respectively. As can be seen in Figure 4, this leads to much smaller collapse factor. In fact, this is in better agreement with cosmological simulations (e.g. Diemand et al. 2007), as the simplification of a constant density is not applied there. However, the half-mass radius still is significantly puffed up in both cases with a cusped profile, similar to our simplified case.

Another caveat in our initial conditions is the fact that the particles are at rest initially. To test this simplifica-

tion we perform a run with a turbulent velocity. The velocity is set to correspond to half the circular velocity, i.e. the potential (see Equation 1 below). Again, the maximum contraction is smaller than in the fiducial case (Figure 4). Still, in the case with mass loss, a significant change in the half-mass radius can be seen. We therefore conclude that the simplifications in our initial conditions do not affect the results strongly.

In order to assess the change of the velocity dispersion, we evaluate the halo potential at a time  $t = 2t_{\text{ff}}$ , i.e. the circular velocity

$$v_{\text{circ}} = \sqrt{\frac{GM}{R}}, \quad (1)$$

where  $G$  is the gravitational constant, and  $M$  is the mass inside the radius  $R$ . This approximation is adequate for small  $R$  where the system has already virialized.

In Figure 5, we plot  $v_{\text{circ}}$  as a function of  $R/R_{\text{hm,ff}}$  where  $R_{\text{hm,ff}}$  is the final half mass radius of the fiducial model (represented by the top black line). We also compare the fiducial case and two models with a 10% mass loss where the mass loss is either confined to the central 20% (the bottom red line) or extended throughout the entire halo (the middle blue line). These results show that mass loss significantly reduces the distribution of  $v_{\text{circ}}$  at all radii to about 3/4 of the case without mass loss.

Finally, the halos here all show a cored density profile, as has already been deduced by Aarseth et al. (1988). This result is in agreement with the finding of most recent observational models which generally favor a cored rather than a cusped profile (e.g. Amorisco & Evans 2012)

#### 4. DISCUSSION

The above models show, that a loss of 10% of the total mass, from the central 20% of the total halo, at a time when the halo has contracted to 1/20 of its original size, is sufficient to reduce the velocity dispersion by  $\sim 20 - 30\%$  and to cause the halo to attain an extended asymptotic structure.

In order to apply these simulated models in the context of Galactic dSphs, it is necessary to convert some of the dimensionless quantities into physical numbers. A straightforward quantity to do the mapping is the mass. By fitting the simulated and observed mass and velocity dispersion distribution, we can establish a characteristic mass, length scaling, and a complete normalization set.

We apply this approach to fit the observed mass profile of the Fornax dSph. We adopt the model parameters inferred from the observed velocity dispersion by Jardel & Gebhardt (2012). They determined its mass to be  $M_{300} = 3.5^{+0.77}_{-0.11} \times 10^6 M_{\odot}$  inside  $R = 300$  pc,  $M_{689} = 3.9^{+0.46}_{-0.11} \times 10^7 M_{\odot}$  inside the projected half-light radius ( $R = 689$  pc) and  $M_{900} = 5.8^{+1.0}_{-0.2} \times 10^7 M_{\odot}$  inside the unprojected half-light radius ( $R = 900$  pc). They also obtained an observed luminosity weighted line-of-sight velocity dispersion  $\sigma = 11.3^{+1.0}_{-1.8} \text{ km s}^{-1}$ .

We set the initial mass of Fornax dSph's entire halo to be  $1.5 \times 10^9 M_{\odot}$  and choose a length scale which matches the observationally inferred mass distribution (Figure 6 left panel). Then, we adopt their value of  $\sigma$  and convert it to a circular velocity  $v_{\text{circ}} = \sqrt{3\sigma^2}$  (Wolf et al. 2010)

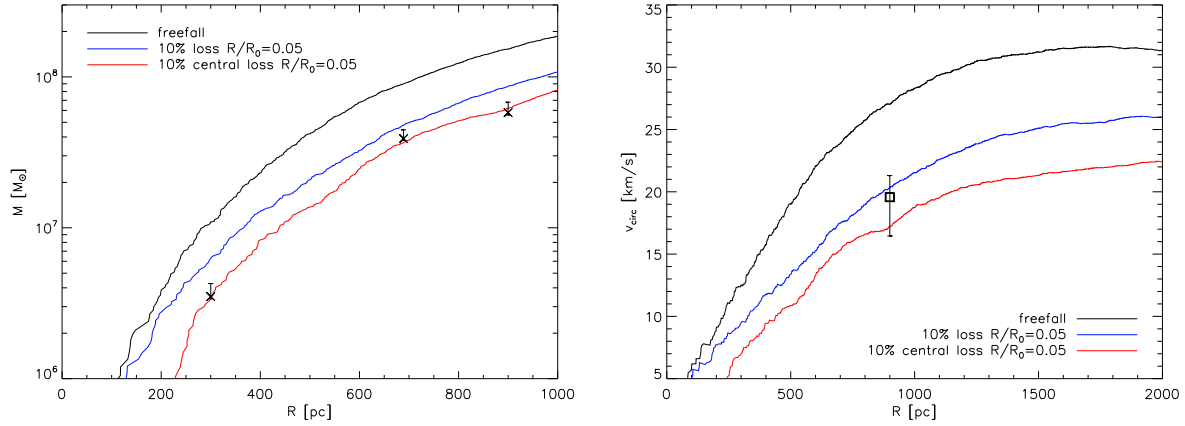


FIG. 6.— Mapping of the simulations to physical quantities. Left: Fitting the mass profile to observations by Jardel & Gebhardt (2012). Right:  $v_{\text{circ}}$ , i.e. the potential, in three selected cases in physical units in comparison with the observed value for Fornax (e.g. Jardel & Gebhardt 2012).

and plot that value at the position of the unprojected half-light radius (Figure 6 right panel).

Although our choice of the initial total mass is somewhat arbitrary, the combined constraint of the observed mass at various physical radii limits the degree of freedom. There are several combinations of mass and radius normalization factors which can fit the data points in the left panel, but they all leave the match between the observations and our profiles in the right panel invariant. Therefore, we do the conversion with an reasonable choice of  $M_{\text{tot}}$ .

Our choice of normalization also gives a timescale,  $t_{\text{ff}} = 2.2$  Gyr, which puts our simulations in a reasonable cosmological context. The length scale is  $R_{\text{hm,ff}} = 9.2$  kpc and the dark matter density is  $\rho_{\text{DM}} \sim 3 \times 10^{-26} \text{ g cm}^{-3}$ . If we use a cosmological baryonic to dark matter ratio, the initial mass of baryonic mass would be  $\sim 2.55 \times 10^8 M_{\odot}$ . Despite the loss of more than 50% of the initial baryonic mass (which corresponds to a loss of  $\sim 10\%$  of the initial total mass), Fornax would still be able to have retained a sufficient amount of baryonic matter to account for its observed stellar mass (Mateo 1998; Jardel & Gebhardt 2012) and some loss of baryonic matter during the subsequent stellar and dynamical evolution.

Our best-fit model requires the mass loss to take place after the half mass radius has contracted by a factor of 20. This collapse factor would reduce the instantaneous infall time scale to  $\sim 10^7$  yr and the average density of the baryonic matter to  $\sim 10^{-22} \text{ g cm}^{-3}$ . These conditions are likely to lead to the onset of star bursts and consequently a strong feedback effect. A detailed investigation will be performed in future work.

## 5. SUMMARY

With the help of a simplified N-body model we are able to show a possible physical cause for the observed puff-up of satellite dSphs around the Milky Way. We propose that the internal star formation feedback during advanced stages of the first infall is sufficient to modify the dark matter potential in order to explain their

modified phase-space density.

A natural next step is to use an SPH scheme to carry out a set of simulations which include a realistic treatment of the loss of baryonic matter. With the SEREN code, we can introduce a more realistic prescription for radiative or supernova driven loss of baryonic matter. For example, the impulsive mass loss prescription may be relaxed with a model for star formation which proceeds on a time scale comparable to the dynamical time scale during the advanced stage of infall. Two types of particles may be used to represent gas and dark matter. Star formation may mostly occur in the baryonic matter concentrated regions. We plan to include the Galactic potential which removes dark matter venturing beyond the dSphs tidal radius. Recent simulations (e.g. Pawlik et al. 2012) include some of these effects and show that the potential is indeed reduced in simulations with feedback (Brooks & Zolotov 2012).

Here, we focus on the physical effect. During the first infall, the particles (dark matter and gas) are on near parabolic orbits. With the removal of a fraction of the mass, preferentially in the centre, the potential is changed sufficiently to make some particles orbits become unbound. We are able to show that e.g. for a loss of 10% of the material in the central 20% of the (current) halo the observed lower value of the potential/the velocity dispersion can be explained within the framework of  $\Lambda$ CDM. The asymptotic dark matter distribution in these dSphs generally has a cored profile.

## 6. ACKNOWLEDGEMENTS

We thank D. Hubber for providing and explaining the SEREN code and J. Bullock for useful conversation. This work was supported in part by NASA grant NNX08AL41G. M.G. acknowledges funding by the Alexander von Humboldt Foundation in the form of a Feodor-Lynen Fellowship and additional funding by the China National Postdoc Fund Grant No. 20100470108 and the National Science Foundation of China Grant No. 11003001 during the initial stages of this project.

## REFERENCES

- Bertschinger, E. 1985, *ApJS*, 58, 39
- Boylan-Kolchin, M., Bullock, J. S., & Kaplinghat, M. 2011, *MNRAS*, 415, L40
- , 2012, *MNRAS*, 422, 1203
- Brooks, A. M., & Zolotov, A. 2012, *ArXiv e-prints*
- Brown, T. M. et al. 2012, *ApJL*, 753, L21
- de Boer, T. J. L. et al. 2012, *A&A*, 539, A103
- Diemand, J., & Kuhlen, M. 2008, *ApJL*, 680, L25
- Diemand, J., Kuhlen, M., & Madau, P. 2007, *ApJ*, 667, 859
- Diemand, J., Kuhlen, M., Madau, P., Zemp, M., Moore, B., Potter, D., & Stadel, J. 2008, *Nature*, 454, 735
- Dong, S., Lin, D. N. C., & Murray, S. D. 2003, *ApJ*, 596, 930
- Ferrero, I., Abadi, M. G., Navarro, J. F., Sales, L. V., & Gurovich, S. 2011, *ArXiv e-prints*
- Fillmore, J. A., & Goldreich, P. 1984, *ApJ*, 281, 1
- Fragile, P. C., Murray, S. D., Anninos, P., & Lin, D. N. C. 2003, *ApJ*, 590, 778
- Gnedin, N. Y., Tassis, K., & Kravtsov, A. V. 2009, *ApJ*, 697, 55
- Governato, F. et al. 2012, *MNRAS*, 422, 1231
- Hubber, D. A., Batty, C. P., McLeod, A., & Whitworth, A. P. 2011, *A&A*, 529, A27
- Jardel, J. R., & Gebhardt, K. 2012, *ApJ*, 746, 89
- Klypin, A., Kravtsov, A. V., Valenzuela, O., & Prada, F. 1999, *ApJ*, 522, 82
- Komatsu, E. et al. 2011, *ApJS*, 192, 18
- Lin, D. N. C., & Faber, S. M. 1983, *ApJL*, 266, L21
- Mateo, M. L. 1998, *ARA&A*, 36, 435
- Moore, B., Ghigna, S., Governato, F., Lake, G., Quinn, T., Stadel, J., & Tozzi, P. 1999, *ApJL*, 524, L19
- Noriega-Crespo, A., Bodenheimer, P., Lin, D. N. C., & Tenorio-Tagle, G. 1989, *MNRAS*, 237, 461
- Pawlik, A. H., Milosavljevic, M., & Bromm, V. 2012, *ArXiv e-prints*
- Purcell, C. W., & Zentner, A. R. 2012, *ArXiv e-prints*
- Rashkov, V., Madau, P., Kuhlen, M., & Diemand, J. 2012, *ApJ*, 745, 142
- Springel, V. et al. 2008, *MNRAS*, 391, 1685
- Tollerud, E. J., Beaton, R. L., Geha, M., Guhathakurta, P., Bullock, J. S., Kalirai, J. S., Kirby, E. N., & Boylan-Kolchin, M. 2012, in *American Astronomical Society Meeting Abstracts*, Vol. 219, American Astronomical Society Meeting Abstracts 219, 201.04
- Wolf, J., & Bullock, J. S. 2012, *ArXiv e-prints*
- Wolf, J., Martinez, G. D., Bullock, J. S., Kaplinghat, M., Geha, M., Muñoz, R. R., Simon, J. D., & Avedo, F. F. 2010, *MNRAS*, 406, 1220